Power Device Losses in Two-Level Converters with Direct Current Controllers for Grid Connected Applications

Jose Ortiz Gonzalez
School of Engineering
University of Warwick
Coventry, United Kingdom
J.A.Ortiz-Gonzalez@warwick.ac.uk

Diego Pérez-Estévez
School of Engineering
University of Vigo
Vigo, Spain
dieperez@uvigo.es

Ruizhu Wu
School of Engineering
University of Warwick
Coventry, United Kingdom
robert.wu.1@warwick.ac.uk

Jesús Doval-Gandoy
School of Engineering
University of Vigo
Vigo, Spain
jdoval@uvigo.es

Phil Mawby
School of Engineering
University of Warwick
Coventry, United Kingdom
p.a.mawby@warwick.ac.uk

Olayiwola Alatise
School of Engineering
University of Warwick
Coventry, United Kingdom
O.Alatise@warwick.ac.uk

***Abstract*—Direct current controllers have been widely used in grid-tied applications and electric drives. Direct controllers select the switching states of the converter without the intervention of a modulation stage. In comparison with PWM based controllers, direct controllers have a faster dynamic response to reference-tracking and disturbance rejection. The different control strategies can affect the total converter losses and device loss distribution; hence it is important to evaluate them when novel control methodologies are presented and compare them to the conventional PWM current controllers. To this end, fully electrothermal simulations can be paramount. Using a grid connected two-level converter, this paper evaluates the power device losses and the resulting junction temperatures excursions of the power semiconductors chips when a direct current controller is used and compares the results to those obtained with PWM controllers working at the same operating points.**

Keywords—Power losses, electrothermal simulation, Grid connected inverter, Direct current controller, PWM controller

I. INTRODUCTION

The use of direct controllers such as Finite-Control-Set Model-Predictive Controllers (FCS-MPC) [1], Direct Power Controllers (DPC) [2], Direct Torque Controllers (DTC) [3], and Finite-Control-Set Noise-Shaping Controllers (FCS-NS) [4] has been facilitated by the increasing computational power and availability of embedded microcontrollers. The operation of direct controllers consists in selecting a switching state of the converter for each sampling period. Direct controllers, compared to the traditional PWM-based linear current controllers, can provide a fast transient response with a lower switching frequency and this can be highly relevant for electric drives and grid-connected converters.

When developing a controller for a grid-tied converter, the main objective is supplying the required active and reactive power while meeting the stringent grid code standards. Control designers focus their efforts on the steady-state harmonic distortion and the dynamic response of the current controller (reference-tracking and disturbance rejection responses). An area of increasing interest is the evaluation the losses on the power semiconductor devices comprising an inverter [5-8] as well as developing control methodologies to improve the thermal performance and reliability of the converter [9-11] .In this sense, fully electrothermal simulations [12] can be very important for understanding the impact of the selected controller on the power device losses and the resulting chip temperature excursions. Some case studies, considering a wind power system are presented in [13, 14]

This paper will evaluate the impact of the current controller on the power device losses and junction temperature excursions of the power devices of a grid-connected three-phase two-level inverter in different operating points. A classic Pulse Width Modulation Proportional Integral controller (PWM-PI) and an FCS-NS controller will be studied using a fast simulation model, based on the measured output currents and gate firing signals. The model can be a useful tool for control engineers and converter designers, assisting them in the tasks of understanding the resulting stresses on the converter and selecting the power semiconductors.

II. PWM-PI AND FCS-NS CONTROLLERS IN TWO-LEVEL GRID CONNECTED CONVERTERS

A. Grid connected converter structure

As mentioned in the introduction, grid connected converters have to provide the required active and reactive power to the grid while keeping a low current harmonic level as defined by the grid standards. A basic representation of a grid-tied inverter (including the control block diagram) is shown in Fig. 1(a), whereas the experimental setup is shown in Fig. 1(b). In this investigation, a classic two-level inverter has been evaluated.

This work was supported in part by the UK EPSRC through the grant reference EP/R004366/1 and the Spanish State Research Agency under Project PID2019-105612RBQ1I00/AEI/10.13039/501100011033.

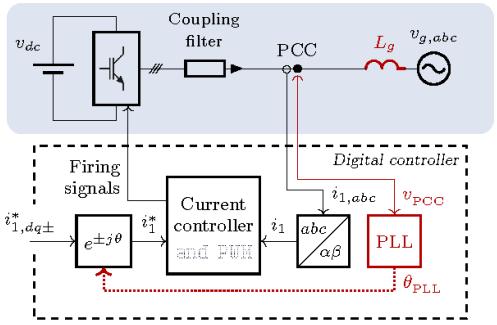

(a)

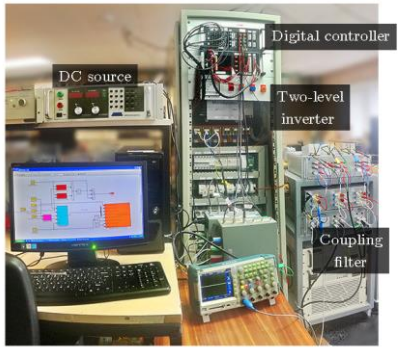

(b)

Fig. 1. (a) Grid connected inverter and control schematic (b) Experimental setup

In the selected experimental configuration, the converter is connected to the grid using an inductive coupling filter (L=0.32 p.u). The control was executed using a digital controller Microautobox 1401, which generates the firing signals of the two-level inverter. A well-known feature of direct controllers is that the average switching frequency depends on numerous factors such as the sampling frequency or the modulation index among others. The modulation index of a converter is determined by the relationship between the DC link voltage and the amplitude of the output voltage of the inverter. For the sake of a fair comparison, in this investigation the DC link voltage has been adjusted to obtain an average switching frequency for the FCS-NS controller approximately equal to the PWM-PI controller.

The direct controller is executed in real-time in an embedded hardware control platform at a sampling frequency of 16kHz, which results in an average switching frequency of 1.8kHz. The PWM-PI controller employs a double update sampling strategy at 3.6kHz, which also results in a 1.8kHz switching frequency. The selected filter inductance value and the switching frequency are commonly employed in low-voltage applications with a two-level voltage source converter (VSC) [15]. The VSC is synchronized with the grid by means of a synchronous reference frame phase-locked loop (PLL) [16].

The embedded control platform is programmed using Simulink programming language, MATLAB scripts, and C code. The embedded controller also provides a large number of analogue input channels that are used to record the experimental waveforms shown in section II.B.

The direct controller selected for the presented comparison is described in [4]. Contrarily to direct controllers that are based on an optimization of a cost function [17, 18], the selected controller uses a linear design with a low computational burden, similar to a state-space PWM-based solution [19]. However, despite it using a completely different theory of operation from MPC designs, the design in [4] produces similar firing signals, as expected from its FCS operation.

B. Experimental Results

In this investigation both PWM-PI and FCS-NS current controllers are evaluated in different operating points, providing the required i_d and i_q currents to the grid. The two operating points evaluated in this paper are: (a) unity power factor (PF) operation or purely active power supplied to the grid (i_d=10 A and i_q=0 A) and (b) STATCOM operation or purely reactive power supplied to the grid (i_d=0 A and i_q=-10A).

The measurements for the purely active power mode are shown in Fig. 2 for the PWM-PI controller and in Fig. 3 for the FCS-NS controller, whereas the measurements for the

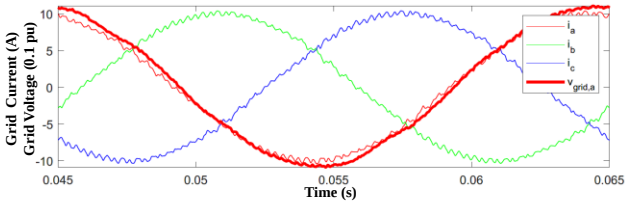

(a)

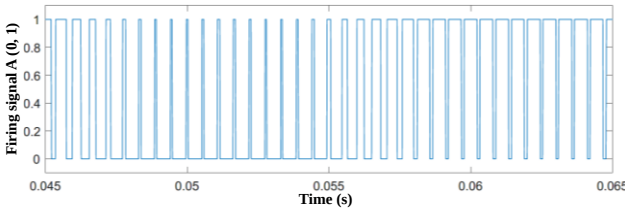

(b)

Fig. 2. Purely active power supplied to the grid. PWM-PI controller (a) Grid currents and phase A voltage (b) Firing Signal phase A

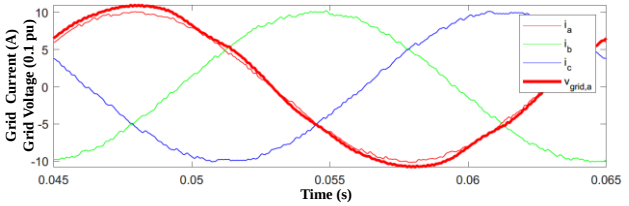

(a)

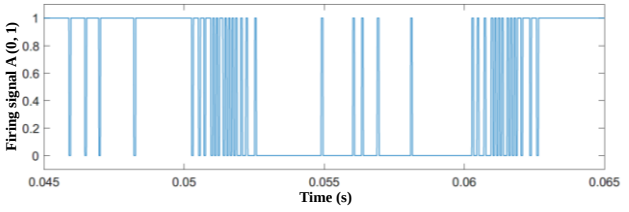

(b)

Fig. 3. Purely active power supplied to the grid. FCS-NS controller (a) Grid currents and phase A voltage (b) Firing Signal phase A

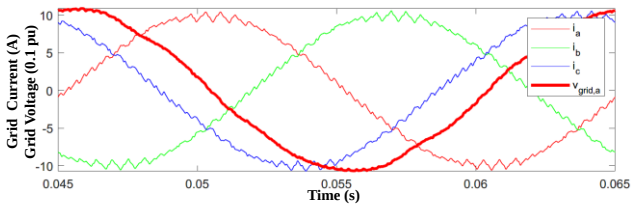

(a)

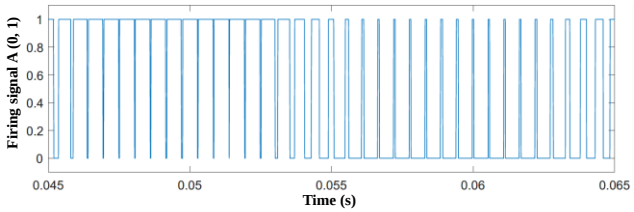

(b)

Fig. 4. STATCOM operation. PWM-PI controller (a) Grid currents and phase A voltage (b) Firing Signal phase A

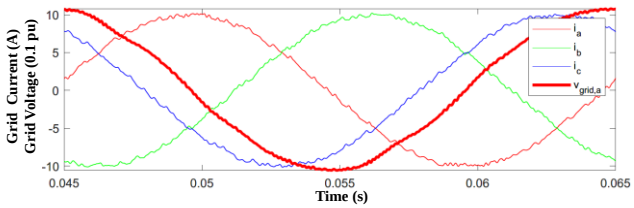

(a)

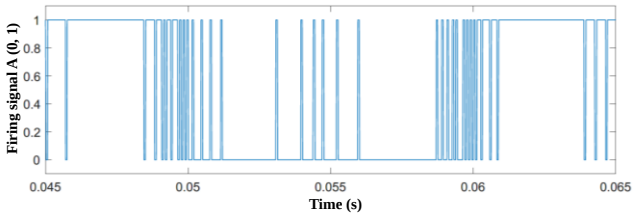

(b)

Fig. 5. STATCOM operation. FCS-NS controller (a) Grid currents and phase A voltage (b) Firing Signal Phase A

STATCOM operation are presented in Fig. 4 for the PWM-PI controller and in Fig. 5 for the FCS-NS controller.

These figures show the output currents/voltages and the gate firing signals (phase B) for one fundamental cycle. As expected, in the case of the unity PF (Fig. 2 and Fig. 3) the grid current is in phase with the grid voltage, whereas a 90° phase shift between voltage and current is observed in the STATCOM operation (Fig. 4 and Fig. 5). It is important to mention that in Fig. 4 and Fig. 5, the current lags 90° because the converter output current has been defined as positive.

Comparing both controllers for the same operating point, it is clearly observed that in the case of the FCS-NS the firing signals include longer periods where the device is ON/OFF. This will affect the balance between switching and conduction losses and the next sections will present an electrothermal model for evaluating the converter loss distribution and resulting junction temperature excursions.

III. Development of the Simulation Model

The development of electrothermal models is an area of increasing interest in power electronics. This type of models enables the investigation of the loss distribution within the devices comprising a converter and the analysis of the resulting junction temperature excursion [12, 20, 21], as well as passive components [22]. As a result of the thermomechanical stresses, the power electronic components degrade, resulting in a reduced lifetime [23, 24]. Hence, it is key to investigate the impact of different mission profiles and operating points on the converter performance.

Defining the switching losses and conduction losses as function of parameters like temperature, load current, and gate voltage is paramount for obtaining an accurate electrothermal model. There are different ways for doing this, including analytical methods, simulation models provided by the manufacturers, look-up tables (LUTs) calibrated using datasheet parameters and LUTs based on experimental characterization. For the investigation presented in this paper, the device selected is a 1200 V/25 A Si IGBT with datasheet reference IKW25T120. The current rating of 25 A is defined for a case temperature of 100 °C. This discrete IGBT is co-packaged with a silicon diode, which is the antiparallel diode in the inverter shown in Fig. 6(a). The conduction losses have been extracted from the device datasheets and the switching energies have been characterized experimentally, using the double pulse test method [12, 25] for a set of currents and temperatures.

The proposed methodology is based on the use of the experimentally measured output currents and gate firing signals of the converter, as measured in the previous section and shown in the conceptual plots in Fig. 6(b) and Fig. 6(c).

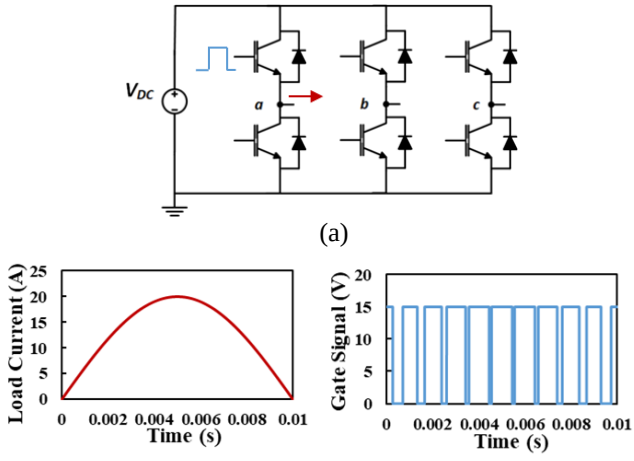

(a) (b) (c)

Fig. 6. (a) 2-level inverter. Conceptual plots for (b) Load current (c) Gate firing signals

The experimental waveforms presented in the previous section were obtained using a converter comprised of different IGBTs/diodes. However, the methodology presented in this in this paper is suitable for evaluating the performance of a converter, assisting converter designers and control engineers in

the task of understanding the loss distribution within the converter, optimizing the power device selection and evaluating the impact on the control strategy on the resulting stresses/junction temperature excursions on the devices.

Using the load current (phase) and the gate firing signals, the resulting conduction and switching losses can be calculated using the loss calculation process [26] shown in Fig. 7 for the conduction losses and the turn-OFF switching losses. Fig. 8 shows the conceptual plots for the conduction losses and switching losses. If the gate firing signal is OFF and the phase current is positive, the current flows through the antiparallel diode of the complementary device (see inverter in Fig. 6(a)). A similar loss calculator is used for the diode, using datasheet-based conduction losses and reverse recovery energies, measured using a double pulse test setup [25]. The 2D LUTs include the electrothermal information extracted from the datasheets and experimental tests, as defined previously.

This process is easy to implement and does not require to measure the current through each device. A typical converter, with a phase current sensor could be used for obtaining the required currents. It is important to mention that the sampling rate of the measured waveforms, especially the gate firing signals, has to be high enough for capturing the short duration ON and OFF gate pulses. In this investigation the sampling time used is 2 µs.

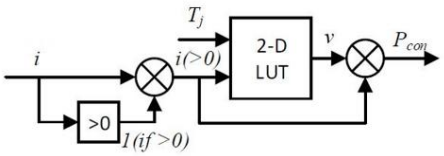

(a)

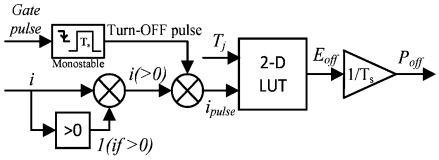

(b)

Fig. 7. Loss calculation method
(a) Conduction losses (b) Turn-OFF switching losses

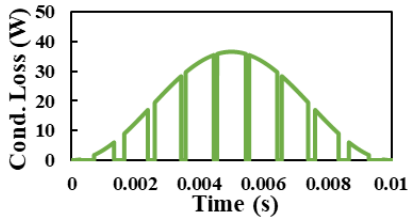

(a)

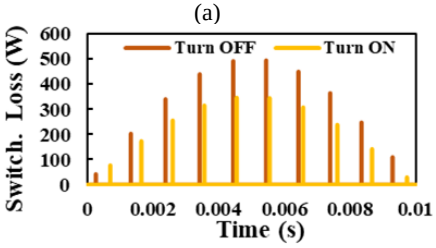

(b)

Fig. 8. Conceptual diagrams for (a) Conduction losses (b) Switching losses

IV. Power Losses And Junction Temperature Analysis

The point of operation of the converter and the control methodology can play a fundamental role on the performance of the converter and the device loss distribution balance. This has been evaluated using the model proposed in the previous section for the FCS-NS and PWM-PI controllers in the two scenarios presented in section II: (a) STATCOM operation (i_d=0 A and i_q=-10 A) and (b) purely active power supplied to the grid (i_d=10 A and i_q=0 A).

The resulting power losses per phase, device loss distribution and device junction temperature excursions are calculated for the purely active power generation and STATCOM operation using the phase output currents and gate firing signals shown in Fig. 2 to Fig. 5. The average switching frequency was fixed to 1800 Hz in both cases, using a DC link voltage of 600 V for the PWM controller and 550 V for the FCS-NS controller. A correction factor was applied to the switching loss LUT, based on the information provided on the datasheet of the device. The thermal network provided by the manufacturer was used for evaluating the device junction temperatures, assuming a fixed case temperature T_{CASE} of 100 °C.

The results for the purely active power case are shown in Fig. 9 for the PWM-PI controller and Fig. 10 for the FCS-NS controller, whereas the results for the STATCOM operation are shown in Fig. 11 and Fig. 12 for the PWM-PI and FCS-NS controller respectively.

Starting the analysis with the purely active power case, the total losses in the converter reduce -11.5% when the FCS-NS controller is used. However, it is also important to evaluate the loss distribution within the power devices comprising the converter. Comparing Fig. 9 and Fig. 10, an increase of the conduction losses on the IGBT is observed when the FCS-NS controller is used.

An interesting observation is that when the FCS-NS controller is used the majority of the switching events occur at low load current values, as observed in Fig. 3. This results in reduced switching losses, which compensate the increased conduction losses when the FCS-NS controller is used. Focusing on the diode, the use of the FCS-NS controller has an obvious impact in the purely active power case, with a clear reduction of the total losses in the diode. This results in reduced junction temperature excursions, as clearly observed in Fig. 10.

Compared with the purely active case, it can be observed that for STATCOM operation the total losses are higher for both control methodologies. In the case of the PWM-PI controller, the losses increase a 5.7% whereas in the case of the FCS-NS controller the increase is 15.5%.

As in the case of the purely resistive load, adopting the FCS-NS controller instead of the PWM-PI in STATCOM mode operation improves the losses in the converter, with a reduction of -3.3%. However, as the results in Fig.12 show, a clear increase of losses in the diode results in larger temperature variations. These increased junction temperature excursions and mean junction temperature have an impact of on the lifetime, as described in [23, 24]. Active temperature control methodologies are proposed for balancing the stresses between the different power devices [11].

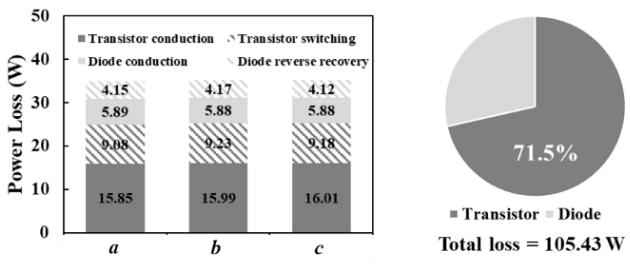

(a)

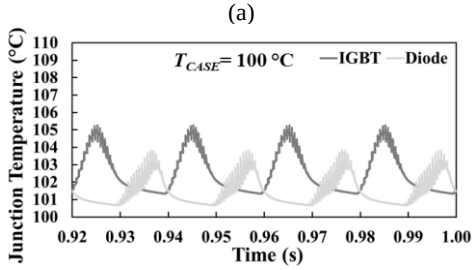

(b)

Fig. 9 PWM-PI Controller. Purely Active Power. (a) Power losses, (b) Transient junction temperatures

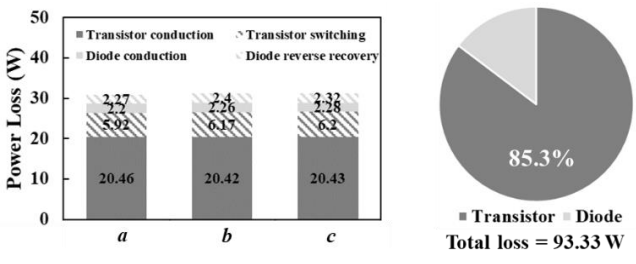

(a)

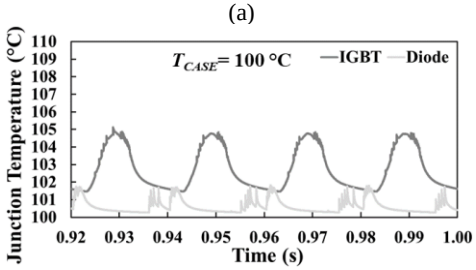

(b)

Fig. 10 FCS-NS Controller. Purely Active Power. (a) Power losses, (b) Transient junction temperatures

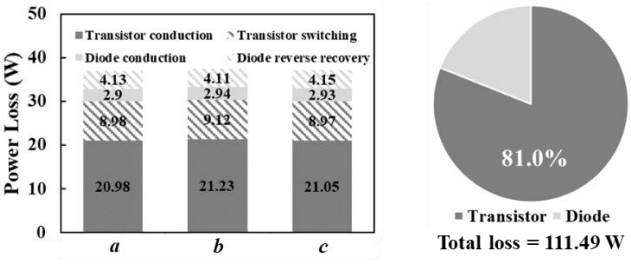

(a)

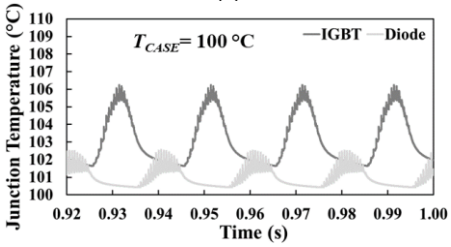

(b)

Fig. 11 PWM-PI Controller. STATCOM operation. (a) Power losses, (b) Transient junction temperatures

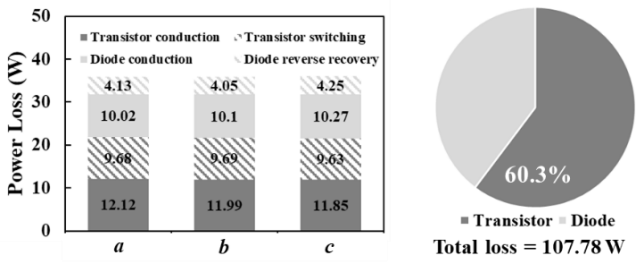

(a)

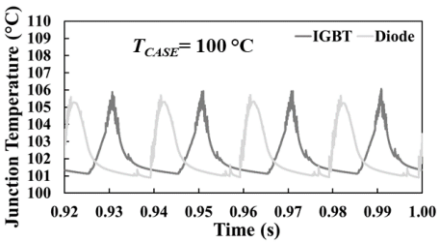

(b)

Fig. 12 FCS-NS Controller. STATCOM operation. (a) Power losses, (b) Transient junction temperatures

V. Conclusions

The impact of direct current controllers on the power device losses and the resulting junction temperatures in the power semiconductors of a two-level Si IGBT grid-connected converter has been evaluated using a fast fully electrothermal model, based on experimentally measured output currents and gate firing signals. The results are compared with those obtained using PWM controllers working at the same operating points and the same average switching frequency. It is shown that FCS-NS controllers can reduce the total losses of the converter: -11.5% in the case of purely active power generation and -3.3% in the case of STATCOM operation. However, when operating as STATCOM the resulting junction temperatures on the diodes are increased.

References

[1] J. Rodriguez *et al*., "Predictive Current Control of a Voltage Source Inverter," in *IEEE Transactions on Industrial Electronics*, vol. 54, no. 1, pp. 495-503, Feb. 2007

[2] R. Portillo, S. Vazquez, J. I. Leon, M. M. Prats and L. G. Franquelo, "Model Based Adaptive Direct Power Control for Three-Level NPC Converters," in *IEEE Transactions on Industrial Informatics*, vol. 9, no. 2, pp. 1148-1157, May 2013

[3] X. Wu, W. Huang, X. Lin, W. Jiang, Y. Zhao and S. Zhu, "Direct Torque Control for Induction Motors Based on Minimum Voltage Vector Error," in *IEEE Transactions on Industrial Electronics*, vol. 68, no. 5, pp. 3794-3804, May 2021

[4] D. Pérez-Estévez and J. Doval-Gandoy, "A Finite-Control-Set Linear Current Controller With Fast Transient Response and Low Switching Frequency for Grid-Tied Inverters," in *IEEE Transactions on Industry Applications*, vol. 56, no. 6, pp. 6546-6564, Nov.-Dec. 2020

[5] M. H. Ahmed, M. Wang, M. A. S. Hassan and I. Ullah, "Power Loss Model and Efficiency Analysis of Three-Phase Inverter Based on SiC MOSFETs for PV Applications," in *IEEE Access*, vol. 7, pp. 75768-75781, 2019

[6] J. S. Artal-Sevil, J. M. Lujano-Rojas, C. Bernal-Ruiz and I. S. Gorrachategui, "Analysis of Power Losses in a Three-Phase Inverter 3L-NPC. Comparison with different PWM Modulation Techniques," 2018 XIII Technologies Applied to Electronics Teaching Conference (TAEE), 2018, pp. 1-9

[7] M. Schweizer, T. Friedli and J. W. Kolar, "Comparative Evaluation of Advanced Three-Phase Three-Level Inverter/Converter Topologies Against Two-Level Systems," in *IEEE Transactions on Industrial Electronics*, vol. 60, no. 12, pp. 5515-5527, Dec. 2013

[8] Z. Davletzhanova, O. Alatise, J. O. Gonzalez, S. Konaklieva and R. Bonyadi, "Electrothermal Stresses in SiC MOSFET and Si IGBT 3L-NPC Converters for Motor Drive Applications," *PCIM Europe 2017; International Exhibition and Conference for Power Electronics, Intelligent Motion, Renewable Energy and Energy Management*, 2017, pp. 1-8.

[9] J. Kuprat, C. H. Van der Broeck, M. Andresen, S. Kalker, R. W. De Doncker and M. Liserre, "Research on Active Thermal Control: Actual Status and Future Trends Special Issue Commemorating 40 years of WEMPEC, 2021," in *IEEE Journal of Emerging and Selected Topics in Power Electronic*s

[10] M. Andresen, K. Ma, G. Buticchi, J. Falck, F. Blaabjerg and M. Liserre, "Junction Temperature Control for More Reliable Power Electronics," in *IEEE Transactions on Power Electronics*, vol. 33, no. 1, pp. 765-776, Jan. 2018

[11] M. Novak, V. Ferreira, M. Andresen, T. Dragicevic, F. Blaabjerg and M. Liserre, "FS-MPC Based Thermal Stress Balancing and Reliability Analysis for NPC Converters," in IEEE Open Journal of Power Electronics, vol. 2, pp. 124-137, 2021

[12] A. Bryant, N. Parker-Allotey, D. Hamilton, I. Swan, P. A. Mawby, T. Ueta, *et al.*, "A Fast Loss and Temperature Simulation Method for Power Converters, Part I: Electrothermal Modeling and Validation," *IEEE Transactions on Power Electronics*, vol. 27, no. 1, pp. 248-257, 2012.

[13] P. Fan, S. Huang, and D. Luo, "Impact of modulation strategies on the lifetime estimation of impedance source inverter in wind power system," *Microelectronics Reliability*, vol. 114,p. 113797, 2020.

[14] J. He, A. Sangwongwanich, Y. Yang and F. Iannuzzo, "Lifetime Evaluation of Power Modules for Three-Level 1500-V Photovoltaic Inverters," *IEEE Applied Power Electronics Conference and Exposition (APEC)*, 2020, pp. 430-435

[15] A. A. Rockhill, M. Liserre, R. Teodorescu and P. Rodriguez, "Grid-Filter Design for a Multimegawatt Medium-Voltage Voltage-Source Inverter," in *IEEE Transactions on Industrial Electronics*, vol. 58, no. 4, pp. 1205-1217, April 2011

[16] X. Wang, M. G. Taul, H. Wu, Y. Liao, F. Blaabjerg and L. Harnefors, "Grid-Synchronization Stability of Converter-Based Resources—An Overview," in *IEEE Open Journal of Industry Applications*, vol. 1, pp. 115-134, 2020

[17] P. Karamanakos, E. Liegmann, T. Geyer and R. Kennel, "Model Predictive Control of Power Electronic Systems: Methods, Results, and Challenges," in *IEEE Open Journal of Industry Applications*, vol. 1, pp. 95-114, 2020

[18] D. Pérez-Estévez and J. Doval-Gandoy, "A Model Predictive Current Controller With Improved Robustness Against Measurement Noise and Plant Model Variations," in *IEEE Open Journal of Industry Applications*, vol. 2, pp. 131-142, 2021

[19] D. Pérez-Estévez, J. Doval-Gandoy, A. G. Yepes, Ó. López and F. Baneira, "Generalized Multifrequency Current Controller for Grid-Connected Converters With LCL Filter," in *IEEE Transactions on Industry Applications*, vol. 54, no. 5, pp. 4537-4553, Sept.-Oct. 2018,

[20] P. Rajaguru, H. Lu, C. Bailey, J. Ortiz-Gonzalez and O. Alatise, "Electro-thermo-mechanical modelling and analysis of the press pack diode in power electronics," *2015 21st International Workshop on Thermal Investigations of ICs and Systems (THERMINIC)*, 2015, pp. 1-6,

[21] L. Ceccarelli, A. S. Bahman, F. Iannuzzo and F. Blaabjerg, "A fast electro-thermal co-simulation modeling approach for SiC power MOSFETs," *2017 IEEE Applied Power Electronics Conference and Exposition (APEC)*, 2017, pp. 966-973,

[22] B. Yao *et al*., "Electro-Thermal Stress Analysis and Lifetime Evaluation of DC-Link Capacitor banks in the Railway Traction Drive System," in *IEEE Journal of Emerging and Selected Topics in Power Electronics*,, Early Access, 2020

[23] U. Choi, F. Blaabjerg and S. Jørgensen, "Study on Effect of Junction Temperature Swing Duration on Lifetime of Transfer Molded Power IGBT Modules," in *IEEE Transactions on Power Electronics*, vol. 32, no. 8, pp. 6434-6443, Aug. 2017

[24] B. Hu *et al*., "Failure and Reliability Analysis of a SiC Power Module Based on Stress Comparison to a Si Device," in *IEEE Transactions on Device and Materials Reliability*, vol. 17, no. 4, pp. 727-737, Dec. 2017

[25] J. O. Gonzalez, R. Wu, S. Jahdi and O. Alatise, "Performance and Reliability Review of 650 V and 900 V Silicon and SiC Devices: MOSFETs, Cascode JFETs and IGBTs," in *IEEE Transactions on Industrial Electronics*, vol. 67, no. 9, pp. 7375-7385, Sept. 2020

[26] R. Wu, J. O. Gonzalez, Z. Davletzhanova, P. A. Mawby and O. Alatise, "The Potential of SiC Cascode JFETs in Electric Vehicle Traction Inverters," in *IEEE Transactions on Transportation Electrification*, vol. 5, no. 4, pp. 1349-1359, Dec. 2019